Understanding the growth mechanisms of TiO2/Al2O3 mixed scales formed on Al-depleted Ti2AlC at 1000–1200 °C

DOI:
10.1016/j.corsci.2022.110393

Document Version
Accepted author manuscript

Understanding the growth mechanisms of TiO_2/Al_2O_3 mixed scales formed on Al-depleted Ti_2AlC at 1000-1200 °C

Xuanzhen Liu [a], Ying Chen [b, c], Ling Li [a], Han Zhang [a], Aihui Huang [a], Xiaohui Fan [a], Xiaofeng Zhao [a], Jie Lu [a, *]

[a] Shanghai Key Laboratory of Advanced High-Temperature Materials and Precision Forming, School of Materials Science and Engineering, Shanghai Jiao Tong University, Shanghai, 200240, China

[b] Department of Materials, The University of Manchester, Manchester M13 9PL, United Kingdom

[c] The Henry Royce Institute, The University of Manchester, Manchester M13 9PL, United Kingdom

Abstract

We present a detailed study of thermally grown oxide scales on a bulk Ti_2AlC material and explore its oxide growth mechanisms at 1000 °C, 1100 °C and 1200 °C, respectively. The oxide scale predominantly consists of an outer TiO_2-rich layer and an inner TiO_2/Al_2O_3 mixed layer. The formation of such a duplex microstructure is caused by the phase transformation from Ti_2AlC to TiC at the scale/substrate interface and the Al depletion due to the formation of impurities. The insufficient supply of Al to scale/substrate interface, together with the competition from growth of TiO_2, prevents formation of a continuous Al_2O_3 scale.

Keywords: Ti_2AlC; Oxidation; Microstructure evolution; Mixed oxide scales

* Corresponding author: Jie Lu (lu-jie@sjtu.edu.cn)

1. Introduction

MAX or $M_{n+1}AX_n$ phases (where M is a transition metal, A is a IIIA or IVA element and X is C or N, n=1, 2, 3) are a new group of ternary compounds with layered, hexagonal structures [1-3]. This new class of materials shares an unusual combination of desirable properties of both ceramics (e.g., high melting point and high creep resistance) and metals (e.g., good electrical and thermal conductivity), which makes them candidate materials for diverse applications [4,5]. Among MAX materials, ternary Ti_2AlC has attracted tremendous attention due to its low density (4.11 g/cm^3), excellent thermal shock resistance, and relatively low coefficient of thermal expansion (CTE) [1,5-7]. Besides, in the crystal structure of Ti_2AlC, the periodic arrangement of Ti_6C octahedral interleaved with a close-packed Al layer endows covalent-ionic Ti-C bonds and metallic Ti-Al bonds [1,7]. The outward diffusion of weakly bonded Al is much easier than that of strongly bonded Ti, which promotes the fast formation of Al_2O_3 during oxidation or corrosion [8,9]. Based on the above mentioned arguments, Ti_2AlC exhibits huge potential for high-temperature structural material applications.

To achieve practical high-temperature applications of Ti_2AlC (or Ti_3AlC, Cr_2AlC), it is of importance to understand its oxidation behavior and evaluate its oxidation performance. To date, the oxidation behavior of Ti_2AlC in the form of bulks, coatings and thin films has been extensively investigated [10-14]. Most studies have shown that Ti_2AlC exhibited an excellent oxidation resistance by forming a continuous external Al_2O_3 scale [6,14-18]. However, a thorough examination of the literature data shows that there are inconsistent findings on oxidation behavior of Ti_2AlC. For example, Barsoum et al. [19,20] found that the oxide scale formed on Ti_2AlC consisted of a mixture of TiO_2 (rutile) and Al_2O_3. Later on, several studies also reported the growth of thick TiO_2/Al_2O_3 mixed scales during oxidation of Ti_2AlC (Ti_3AlC_2) and attributed this behavior to the anisotropy of the Ti_2AlC (Ti_3AlC_2) crystal structure and the large grain size (ranging from 20 to 100 μm) [17,18,21,22]. In addition, the mixed oxide scale is also found in oxidation of Cr_2AlC, suggesting that the growth of the TiO_2/Al_2O_3 mixed scale might be a common issue in Al containing MAX phase [23]. Such mixed oxide

scales are fast-growing and detrimental to the oxidation performance, finally causing the rapid metal consumption and failure of Ti_2AlC. The inconsistent results indicated that the microstructure of the oxide scales formed on Ti_2AlC and the resulting oxidation performance were quite different. Therefore, understanding the growth mechanisms of the TiO_2/Al_2O_3 mixed scale on Ti_2AlC is vital for optimizing or improving its oxidation performance. However, the oxidation behavior related to the TiO_2/Al_2O_3 mixed scale for Ti_2AlC lacks systematic study and remains unclear.

The objective of this work is to clarify the growth mechanism of the TiO_2/Al_2O_3 mixed scale formed on Ti_2AlC. Bulk Ti_2AlC samples are prepared by consolidating the commercial Ti_2AlC powder using the spark plasma sintering (SPS) technique. Three temperatures, including 1000 °C, 1100 °C and 1200 °C, are chosen to understand the temperature effect on oxidation behavior. The microstructural evolution and oxidation behavior of Ti_2AlC are studied in detail. The results are discussed comprehensively to probe the underlying oxidation mechanisms.

2. Experimental procedure

2.1 Materials and sample preparation

The commercially available Ti_2AlC powder with a particle size range of 5-20 μm was used to fabricate Ti_2AlC samples. The powder was packed in a boron nitride coated graphite mound and then sintered at 1250 °C for 10 min in vacuum (10^{-3} Pa) using SPS. During sintering, the pressure was kept at 50 MPa. The heating rate was set to be 80 °C/min and the cooling time to room-temperature was about 30 min. The as-sintered materials were 30 mm in diameter and 10 mm in thickness. The materials were ground on SiC papers to remove the residual graphite and boron nitride.

2.2 Isothermal oxidation test

The as-sintered Ti_2AlC materials were cut into rectangular plates ($10\times10\times3$ mm^3) using a SiC abrasive cutting blade in a precision cut-off machine (Accutom 5, Struers). The sample surface was ground and polished to a mirror finish. The isothermal oxidation tests were performed at 1000 °C, 1100 °C and 1200 °C in a chamber furnace in static

air, respectively. The samples were placed next to a thermocouple in the center of the chamber furnace. After required exposure time, samples were removed from the furnace and air-cooled to room temperature.

2.3 Characterization

The phase composition of as-sintered and oxidized samples was studied by an X-ray diffractometer (XRD, Ultima IV, Rigaku, Japan) with Cu Kα radiation (0.15406 nm) at 30 kV and 300 mA (0.02° step size, a scanning rate of 2 °/min). Photoluminescence piezospectroscopy (PLPS) was applied to characterize the crystallographic phases of the thermally grown Al_2O_3. PLPS was carried out on a confocal Raman microprobe (LabRAM HR, Horiba Jobin Yvon, France) fitted with a 532 nm Nd:YAG laser. The surface and cross-sectional morphologies of oxidized samples were examined by filed-emission scanning electron microscopy (SEM, Mira3, TESCAN, Czech) fitted with an energy-dispersive spectroscopy system (EDS, Aztec X-Max80, Oxford Instruments). To further analyze the phase composition of the as-sintered samples and oxides, thin lamellas from the selected areas were prepared by a focused ion beam (FIB, GAIA3, TESCAN, Czech) and analyzed using a scanning transmission electron microscope (STEM, TALOS F200X, FEI, USA) equipped with an EDS system (XIS Ultra DLD, Kratos, Japan).

3. Results

3.1 Microstructure of the Ti_2AlC powder and as-sintered sample

Fig. 1a shows XRD patterns obtained from Ti_2AlC powder and as-sintered samples. The phase composition of both powder and as-sintered samples is predominantly Ti_2AlC. The sharp, high intensity peaks of Ti_2AlC suggest that a good crystallization is achieved. In addition, there is a change in the relative intensity of diffraction peaks between powder and as-sintered material, which suggests that there is some degree of texture in the bulk material. However, the texture may not be significant since the strongest peak remains (103), which is significantly different from the highly textured Ti_2AlC materials reported in previous work [21] where (00l) and (hk0) are the two

prominent diffraction peaks for the top and side surface, respectively. Although only Ti_2AlC is identified in XRD patterns, SEM observations of the polished surface show that there are patchy areas with different contrasts from the Ti_2AlC matrix (bright contrast). The area with dark contrast is identified as α-Al_2O_3 by EDS and PLPS analysis (Fig. 1b-d). To determine the structure and chemical composition of the areas with gray contrast, a FIB lamella across the interfaces between the Ti_2AlC matrix and the grey contrast was extracted (similar as the blue rectangle in Fig. 1b). Based on the STEM-EDS analysis (Fig. 1e) and the corresponding selected-area diffraction patterns (SADPs, Fig. 1g and f), it can be concluded that Area f (grey contrast) and g (bright contrast) are $TiAl_3$ phase ($L1_2$ structure) and Ti_2AlC phase, respectively. Furthermore, the volume fractions of $TiAl_3$ and Al_2O_3 are 5.3 ± 0.6% and 2.0 ± 0.2%, respectively, as quantified by image analysis in Fig. 1h.

3.2 Growth kinetics of the oxide scales

Fig. 2a shows the dependence of the oxide thickness on oxidation time at three temperatures. It can be seen that the thickness increases rapidly with oxidation time in the investigated temperature range. Even at 1000 °C, the thickness after 48 h reaches about 330 ± 25 μm, which is significantly larger than that in reported works [3,6]. Based on Wanger's theory, when diffusion through the oxide scale is the rate-determining step, the parabolic oxidation model is commonly utilized to describe oxidation kinetics, which is given by [20]:

$$x^2 = 2k_p t \quad (1)$$

Where x is the oxide scale thickness, t is the oxidation time, k_p is the parabolic rate constant. Fig. 2b plots the oxide scale thickness as a function of square root of oxidation time. For samples oxidized at 1000 °C and 1100 °C, high correlation coefficient values (R^2) indicate oxidation kinetics obeys the parabolic law over this temperature range. Meanwhile, the parabolic rate constants at 1000 °C (3.0×10^{-9} cm^2 s^{-1}) and 1100 °C (3.2×10^{-8} cm^2 s^{-1}) are comparable to the values reported by Yu. et al. [17] and Barsoum et al. [19,20].

Interestingly, it is worth noting that two distinct stages can be seen from fitting results at 1200 ℃ in Fig. 2b. Stage I shows a relatively higher parabolic rate constant than that in Stage II, suggesting that the two stages have different oxidation kinetics. Specifically, at the early stage of oxidation at 1200 ℃, the oxide scale grows rapidly and increases to 210 ± 15 μm within 1 h (Fig. 2), while oxidation kinetics exhibits a parabolic mode. However, after long-term oxidation at 1200 ℃, the oxidation rate decreases based on the parabolic fitting of the experimental data in Fig. 2b, which is attributed to the formation of a continuous and slowly growing Al_2O_3 layer in contact with substrate, as discussed later in Fig. 6e.

Furthermore, an Arrhenius-type plot is also given in Fig. 3, where $\ln(k_p)$ is plotted as a function of $1/T$. The function is described as [24]:

$$k_p = k_0 \exp^{(-\frac{Q}{RT})} \quad (2)$$

Where k_0 is a constant, R is the gas constant in kJ/(mol·K), T is the absolute temperature, and Q is the effective activation energy in kJ/mol. The value of the effective activation energy for oxidation is calculated using the data from Fig. 2b. Since the change of oxidation kinetics and the thickening of oxide scales mainly occur within 1 h at 1200 ℃, the k_p value at Stage I is selected for Arrhenius-type plot. The slope of the linear fitting yields a value for Q of 252 kJ/mol. The grain boundary diffusion energy for oxygen in Al_2O_3 is about 380 kJ/mol [16,24]. Thus, the lower Q value indicates that the oxidation rate-controlling step is different, which will be further discussed in later section.

3.3 Phase composition and morphology of the oxide scales

3.3.1 Phase composition

Surface appearance and phase composition of the oxide scales formed after oxidation are presented in Fig. 4. It should be mentioned that XRD analysis was conducted from the sample surface. Based on the linear attenuation coefficient of the oxide compositions, the penetration depth of the X-ray through oxides scales under experiment conditions is about dozens of microns. Consequently, the XRD results show

the phase compositions of samples near the surface region. The sample surface after 6 h oxidation at 1000 °C and 1100 °C turns orange and maintains this color after 48 h oxidation (Fig. 4a). Similar results are also reported in previous work [18]. However, surface color is slightly different after oxidation at 1200 °C, suggesting a change in phase composition of the oxide scale. XRD analysis in Fig. 4b and c shows the oxide scale formed at 1000 °C and 1100 °C is dominated by TiO_2 (rutile) with a small amount of Al_2O_3. Meanwhile, Al_2TiO_5 peaks are detected after 6 h and 48 h oxidation at 1100 °C, which results from the reaction between Al_2O_3 and TiO_2. At 1200 °C, Al_2O_3 peaks almost disappear, while TiO_2 and Al_2TiO_5 are clearly detected (Fig. 4b and c). Although previous studies reported that Al_2TiO_5 was identified at temperatures above 1200 °C [3,6], it is expected that Al_2TiO_5 can be formed at 1100 °C since the formation and decomposition processes of it occur simultaneously in a temperature range from 1100 to 1300 °C [25]. Besides, it should be also noted that the peak intensity of Al_2TiO_5 at 1100 °C is much stronger than that at 1200 °C in Fig. 4b, which could be attributed to the anisotropic growth.

3.3.2 Morphology evolution

Fig. 5 displays the typical surface morphology of samples oxidized at 1000 °C, 1100 °C and 1200 °C. For all samples, the scale surface is uneven. Under the secondary electron mode (SE), elongated granules with sharp edges and smooth facets are seen on the surface at 1000 °C (pointed by white arrows in Fig. 5a) [26,27]. From the corresponding backscattered electron (BSE) image in Fig. 5b, no obvious contrast variation can be observed, which suggests a predominant TiO_2 formation at the scale surface. An increase in oxidation temperature from 1000 °C to 1100 °C results in a higher diffusion rate of Ti to the surface, which is translated to a higher diffusion flux for feeding TiO_2 granules growth (50 ± 5 μm in length in Fig. 5c and d). Similar surface morphology and contrast features are also observed at 1200 °C (Fig. 5e and f). However, the size of elongated granules is decreased in length.

In order to further understand the oxidation behavior of as-sintered Ti_2AlC samples, the cross-sectional microstructure of the oxide scale is presented in Fig. 6. Combined with

the EDS and XRD results, it is clear that the oxide scale is mainly composed of a mixture of TiO_2 (bright contrast) and Al_2O_3 (dark contrast) at three oxidation temperatures (Fig. 6). In addition, EDS analysis taken from the dark grey region (pointed in white arrows in Fig. 6e) shows that they are composed of Ti, Al and O. Quantitative EDS analysis indicates that the atomic ratio of Ti/Al is close to 1:2, suggesting that the dark gray region is Al_2TiO_5. However, Al_2TiO_5 is not discussed in the oxide scale due to its lower content compared with TiO_2 and Al_2O_3. The oxide scale is 330 ± 25 μm at 1000 °C, but reaches 1034 ± 50 μm at 1100 °C. When the temperature increases to 1200 °C, the thickness of the oxide scale decreases to 580 ± 20 μm. Besides, one prominent feature of the oxide scale formed at 1000 °C and 1100 °C is a three-layer structure (Fig. 6a and c), which consists of a top TiO_2-rich layer with minor Al_2O_3, an intermediate Al_2O_3-rich layer and a thick TiO_2/Al_2O_3 mixed layer in contact with the substrate [20,26]. However, an increase of oxidation temperature from 1100 °C to 1200 °C results in formation of a continuous Al_2O_3 layer underneath the TiO_2/Al_2O_3 mixed layer (Fig. 6e and f). The occurrence of the Al_2O_3 layer decreases the total Ti flux reaching to the surface with oxidation time due to the low diffusivity of Ti through Al_2O_3 [13]. The decreased Ti flux might be the reason for the smaller TiO_2 size in Fig. 5c.

From the gas/scale interface to the scale/substrate interface, the microstructure of the oxide scale shows a transition from Ti-rich oxide to Al-rich oxide, which indicates that selective oxidation of Al occurs on Ti_2AlC. Based on quantitative analysis of Fig. 6a, c and e, the volume fraction of Al_2O_3 in TiO_2/Al_2O_3 layer is 28 ± 1%, 32 ± 2% and 40 ± 1% at 1000 °C, 1100 °C and 1200 °C, respectively. Moreover, an obvious contrast variation across the scale/substrate interface can be observed in Fig. 6a and c. EDS mapping in Fig. 6b reveals that these white layers are Al-depletion areas. The thickness of the Al-depletion layer increases from 102 ± 12 μm (1000 °C) to 383 ± 40 μm (1100 °C), resulting from a fast consumption of Al [13,27-29]. It is also observed in Fig. 7 that the thickness of Al-depletion layer attains 72 ± 8 μm after 30 min oxidation at 1200 °C.

4. Discussion

4.1 Phase evolution during Ti_2AlC oxidation

Based on the findings from Arita et al. [30] and Haul et al. [31], the diffusion rate of O in TiO_2 is predominantly determined by the oxygen vacancy concentration. The formation of TiO_2 provides fast passages for inward diffusion of O and outward diffusion of Ti [20,32]. In addition, their results also show that the activation energy for diffusion of O in TiO_2 (rutile) is 242-246 kJ/mol (877-1177 °C), which is comparable to that for Ti_2AlC oxidation. Thus, the inward diffusion of O through TiO_2 plays an important role during the oxidation of Ti_2AlC in this study.

Simultaneously, an Al-depletion layer is formed at the interface due to the fast outward diffusion of Al. Fig. 8 shows high magnification BSE images and the corresponding EDS analysis. Since grain boundaries are preferred diffusion paths for Al, it can be seen that Al-depletion regions form along the edge of Ti_2AlC grain boundaries (highlighted by solid lines in Fig. 8a and c) [33]. But after oxidation for longer time at higher temperatures (Fig. 8b and d), the distribution of Al at grains and grain boundaries shows no apparent difference, indicating that Al in the inner parts of Ti_2AlC grains is also consumed (marked by dashed lines). Moreover, some Al-rich areas are identified in Fig. 8b and d, suggesting that Al_2O_3 forms around the original Ti_2AlC grains and shows inhomogeneous distribution (dark contrast marked by dashed lines). It is previously reported that more Al_2O_3 can form on the Ti_2AlC surface if the surface is perpendicular to the basal plane since Al diffusion along the basal plane is faster [17,21]. In contrast, less Al_2O_3 tend to form if the surface is parallel to the basal plane because of the slow Al diffusivity in the c-axis direction [21]. Thus, it is expected that the distribution of Al_2O_3 results from the variation in orientations of Ti_2AlC.

In order to further analyze the oxidation process of Ti_2AlC and confirm the origin of dark contrasts in Fig. 8, a thin lamella is extracted by FIB in the blue area in Fig. 8d and TEM analysis of the lamella is presented in Fig. 9. It is clearly indicated through HAADF-STEM image combined with EDS maps that three characteristic regions can

be identified. Region b is enriched with Al and O, which is marked by dashed lines in Fig. 9a and the corresponding mapping of Al. Region c is enriched with Ti and C and contains a lower Al content (marked by solid lines). Region d is enriched with Ti and C. Combined with the SADPs in Fig. 9b-d, the materials in region b, c and d are identified as Al_2O_3, Ti_2Al_xC and TiC, respectively.

Moreover, the phase transformation from Ti_2AlC to TiC results in a severe volume shrinkage, which explains the formation of elongated holes as reported in previous studies (pointed by white arrows in Fig. 9a) [1,14,34]. No evidence of Ti and O enrichment areas (e.g., TiO_2) is detected in EDS mapping. Therefore, the oxidation process of Ti_2AlC can be divided by three steps: (1) the fast diffusion of Al favors the Al_2O_3 formation at grain boundaries; (2) meanwhile, Ti_2Al_xC is decomposed into TiC by forming the porous structures due to the outward diffusion of Al; (3) thereafter, TiC is further oxidized into TiO_2.

4.2 Effect of impurities on Al-depleted Ti_2AlC oxidation

Previous studies have indicated that a protective Al_2O_3 scale formed on highly pure Ti_2AlC materials [3,6,16,28]. However, the as-sintered samples in this work are composed of a Ti_2AlC phase and two other impurity phases, as presented in Fig. 1 (5.3 ± 0.6% $TiAl_3$ and 2.0 ± 0.2% Al_2O_3). Thus, a plausible explanation for the different oxidation behavior is the presence of impurities involved in Ti_2AlC sintering. Generally, impurities such as Al_2O_3 and Ti_xAl_y (Ti_3Al or $TiAl_3$) might occur in the process of Ti_2AlC preparation, which is detrimental to the oxidation of Ti_2AlC by depleting the Al reservoir in the Ti_2AlC matrix. Quantitative EDS point analysis in Fig. 1e shows that the atomic ratio of Ti: Al: C in the Ti_2AlC matrix is 2: 0.87: 0.91, which suggests an Al loss by 8% comparing with the ideal 2:1:1. The Al loss in Ti_2AlC can further reduce the supplement of Al to the interface during oxidation. Subsequently, the supplement of Al might be insufficient to compensate the consumption of Al for maintaining the growth of Al_2O_3. With the inward diffusion of oxygen, the non-protective TiO_2 forms.

Besides, from the thermodynamic point of view, the Al content has a significant

influence on its activity at high temperatures [35]. Due to the presence of $TiAl_3$ and Al_2O_3 in as-sintered samples, the decreased Al content can further lower the Al activity in Ti_2AlC. Therefore, the selected oxidation of Al cannot be fully realized to form a protective Al_2O_3 scale, which in turn results in the competitive growth of TiO_2 and Al_2O_3 at the same time. Based on the discussion mentioned above, the growth of the TiO_2/Al_2O_3 mixed scale is predominantly attributed to the Al loss in Ti_2AlC due to the formation impurity phases. Therefore, it will be crucial to understand the growth mechanisms of TiO_2/Al_2O_3 mixed scale once the growth of a protective Al_2O_3 scale cannot be supported.

4.3 Growth mechanism of the TiO_2/Al_2O_3 mixed scale

The thick TiO_2/Al_2O_3 mixed scale is formed on the Al-depleted Ti_2AlC at three temperatures. The appearance of TiC phase and Al-depleted areas at the scale/substrate interface reveal that Ti_2AlC has transformed to TiC due to the rapid diffusion of Al. This is related to the formation of the mixed oxide scale.

It is clear that during oxidation Al diffuses out to form Al_2O_3, resulting in the decomposition of Ti_2AlC to TiC. With the progressive inward diffusion of oxygen, TiC is further oxidized into TiO_2 [27,36]. Simultaneously, Ti begins to diffuse out from the Al-depletion areas along grain boundaries [36]. The outward diffusion of Ti feeds the growth of TiO_2, which has been discussed in Fig. 3. Based on the results mentioned above, chemical reactions occur during Ti_2AlC oxidation, which is similar to Ti-Al alloy oxidation. The reactions are summarized as follows:

$$2Al(s) + \frac{3}{2}O_2(g) = Al_2O_3(s) \quad (3)$$

$$Ti(s) + O_2(g) = TiO_2(s) \quad (4)$$

$$TiC(s) + 2O_2(g) = TiO_2(s) + CO_2(g) \quad (5)$$

The corresponding Gibbs free energy change of each reaction can be estimated from the following equations [37,38]:

$$\Delta G(\text{kJ/mol}) = -1688.1 + 0.327T \quad (6)$$

$$\Delta G(\text{kJ/mol}) = -943.5 + 0.179T \quad (7)$$

$$\Delta G(\text{kJ/mol}) = -1154.9 + 0.170T \quad (8)$$

Note that the Gibbs free energy changes per mol oxygen at 1000-1200 °C are negative, which indicates all these chemical reactions can occur spontaneously. To further determine the most likely thermodynamic stable oxides during oxidation, the oxygen equilibrium pressure for each reaction is calculated. For the formation of Al_2O_3, the equilibrium constant (K) is formulated as [35]:

$$\Delta G = -\mathrm{R}T\ln K \quad (9)$$

$$K = \frac{a_{Al_2O_3}}{a_{Al}^2 P_{O_2}^{3/2}} \quad (10)$$

For the following calculations, an assumption is made that the activity of Al_2O_3 (as pure oxide) is one. Then, combining Eqs. (9) and (10), the oxygen equilibrium pressure for reaction (3) is given by:

$$\ln P_{O_2} = \frac{2\Delta G}{3\mathrm{R}T} - \frac{4\ln a_{Al}}{3} \quad (11)$$

Correspondingly, the oxygen equilibrium pressure for reactions (4) and (5) are expressed as follows:

$$\ln P_{O_2} = \frac{\Delta G}{\mathrm{R}T} - \ln a_{Ti} \quad (12)$$

$$\ln P_{O_2} = \frac{\Delta G}{2\mathrm{R}T} + \frac{\ln P_{CO_2}}{2} \quad (13)$$

Then, if the corresponding Gibbs free energy change in Eqs. (6) to (8) is introduced into Eqs. (11) to (13), the graphic representation of the oxygen equilibrium pressure as a function of the reciprocal absolute temperature is given in Fig. 10. It can be observed that the oxygen equilibrium pressure of Al/Al_2O_3 is several orders of magnitude lower than that of Ti/TiO_2. Thus, the Al_2O_3 and TiO_2 can grow simultaneously due to the high oxygen partial pressure at the initial stage of oxidation (Fig. 11a). Since the growth rate of TiO_2 is much faster than that of Al_2O_3, TiO_2 outgrows Al_2O_3 and forms the outermost TiO_2 layer (Fig. 11b) [11,14,26]. As discussed in Section 4.1, TiO_2 can provide the fast

passages for penetration of oxygen. The resulting oxygen partial pressure at the scale/substrate interface can be above the equilibrium pressure (marked by Area A in Fig. 10a). It should be noted that reactions (3) to (5) will only occur when the oxygen partial pressure is above the equilibrium state. Consequently, the growth of TiO_2 does not stop, while a discontinuous Al_2O_3 forms underneath the outermost TiO_2 layer (Fig. 11b). As the oxidation proceeds, the fast outward diffusion of Al leads to the formation of an Al-depletion layer, which finally results in the phase transformation from Ti_2AlC to TiC near the interface (Fig. 11c and d). In addition, a large number of visible pores formed in this layer (Fig. 4) provides channels for oxygen diffusion to the interface. Once the oxygen partial pressure is within Area B or A in Fig. 10a, the oxidation of TiC occurs and dominates the oxidation process, thus forming the TiO_2/Al_2O_3 mixed layer.

To explain why a continuous Al_2O_3 layer forms underneath the mixed oxide scale at 1200 °C, it is necessary to determine the activity of Al and Ti in Ti_2AlC. However, such data are unavailable in open literatures. For simplicity, the activity of Al and Ti in Ti-Al system is used for further calculations. Based on the existing thermodynamic data reported in the literature [35], the variation of the oxygen equilibrium pressure at 1200 °C is plotted in Fig. 10b. The results are similar at 1000 °C and 1100 °C, but oxygen equilibrium pressure is much lower than that at 1200 °C. Thus, the graphical presentation at 1000 °C and 1100 °C is omitted. At 1200 °C, a higher Al activity leads to an increase in Al_2O_3 volume fraction in TiO_2/Al_2O_3 mixed layer (Section 3.3.2). The formation of an Al_2O_3 enriched layer can further decrease the oxygen partial pressure as Al_2O_3 is an effective oxygen diffusion barrier (Fig. 11d). Once the oxygen partial pressure is lower than the equilibrium pressure in TiC/TiO_2 but higher than that in Al/Al_2O_3 (pointed at Area C in Fig. 10b), TiO_2 stops growing but Al_2O_3 can continue to grow and form a continuous layer (Fig. 11e). Furthermore, if the effect of carbon on the activity of Al and Ti is taken into consideration, the strong Ti/C bonding would decrease the activity of Ti, which in turn results in a relatively higher activity of Al [6]. Based on Eq. (11), it can be concluded that the equilibrium oxygen pressure will decrease with increasing a_{Al}. Thus, the higher activity of Al can cause the downward movement of the

Al/Al_2O_3 line in Fig. 10b, which facilitates the formation of Al_2O_3 at 1200 °C. At 1000 °C and 1100 °C, the outward diffusion of Al results in an Al-depletion layer and thus the insufficient supply of Al to the interface. Note that a decreasing Al content can reduce the activity of Al (a_{Al}) in a certain range, which would consequently increase the equilibrium oxygen pressure of Al/Al_2O_3. This reduces the gap between the Al/Al_2O_3 and TiC/TiO_2 lines as shown in the left region along the vertical line in Fig. 10b. Thus, the competition between growth of Al_2O_3 (from Al in Ti_2AlC) and TiO_2 (from TiC) occurs in case of high oxygen partial pressure.

5. Conclusions

In this study, the growth mechanism of TiO_2/Al_2O_3 mixed oxide scales formed on the Al-depleted Ti_2AlC is investigated between 1000 °C and 1200 °C. Thermodynamic calculations are performed to understand the oxidation behavior related to this mixed oxide scale. The following conclusions can be drawn:

(1) The as-sintered sample consists of an Ti_2AlC phase and two major impurity phases (Al_2O_3 and $TiAl_3$). The high content of Al_2O_3 and $TiAl_3$ (7.3% in volume fraction) decreases the Al content by 8 at.% in the Ti_2AlC matrix, which leads to the insufficient supplement of Al during oxidation.

(2) A thick TiO_2/Al_2O_3 mixed oxide scale forms at 1000 °C, 1100 °C and 1200 °C. The scale mainly consists of an outer continuous TiO_2 layer (rutile) with minor Al_2O_3, and a TiO_2/Al_2O_3 mixed layer. However, a continuous inner Al_2O_3 layer forms at the scale/substrate interface after long-term oxidation at 1200 °C.

(3) The oxidation kinetics obeys a parabolic law between 1000 °C and 1200 °C. Additionally, the oxidation rate of as-sintered samples at 1200 °C decreases after 1 h oxidation, due to the formation of a continuous Al_2O_3 layer. Therefore, the oxidation kinetics at 1200 °C shows two different stages.

(4) The fast diffusion of Al leads to the formation of Al_2O_3 at grain boundaries and the decomposition of Ti_2Al_xC to TiC, while the volume shrinkage induced by the phase decomposition causes the formation of elongated holes.

(5) The occurrence of the large Al-depletion layer at 1000 ℃ and 1100 ℃ triggers the insufficient supply of Al to the oxide scale, and decreases the Al content at the interface, which further results in an increase in oxygen partial pressure. Thus, the competition of Al_2O_3 (from Al in Ti_2AlC) and TiO_2 (from TiC) at a higher oxygen partial pressure makes it preferential to establish a TiO_2/Al_2O_3 mixed scale. However, both the high Al activity and low oxygen partial pressure caused by the high-volume fraction of Al_2O_3 at 1200 ℃ facilitate the formation of a continuous Al_2O_3 layer at the scale/substrate interface.

Data availability

The raw/processed data required to reproduce these findings can be shared upon reasonable requests.

Acknowledgment

This work was supported by Shanghai Sailing Program (No. 22YF1419200) and National Natural Science Foundation of China (No. 51971139 and No. 52102072).

References

[1] M.W. Barsoum, The $M_{n+1}AX_n$ phases: A new class of solids: thermodynamically stable nanolaminates, Prog. Solid State Chem. 28 (1-4) (2000) 201-281.

[2] P. Eklund, M. Beckers, U. Jansson, H. Högberg, L. Hultman, The $M_{n+1}AX_n$ phases: Materials science and thin-film processing, Thin Solid Films, 518 (8) (2010) 1851-1878.

[3] B. Cui, D.D. Jayaseelan, W.E. Lee, Microstructural evolution during high-temperature oxidation of Ti_2AlC ceramics, Acta Mater. 59 (10) (2011) 4116-4125.

[4] Z. Zhang, X.M. Duan, D.C. Jia, Y. Zhou, S.Y.D. Zwaag. On the formation mechanisms and properties of MAX phases: a review. J. Eur. Ceram. Soc. 41 (2021) 3851-3878.

[5] X.H. Wang, Y.C. Zhou, Layered machinable and electrically conductive Ti_2AlC and Ti_3AlC_2 ceramics: A review, J. Mater. Sci. Technol. 26 (5) (2010) 385-416.

[6] X.H. Wang, Y.C. Zhou, High-temperature oxidation behavior of Ti_2AlC in air, Oxid. Met. 59 (2003) 303-320.

[7] N.J. Lane, S.C. Vogel, E.a.N. Caspi, M.W. Barsoum, High-temperature neutron diffraction and first-principles study of temperature-dependent crystal structures and atomic vibrations in Ti_3AlC_2, Ti_2AlC, and $Ti_5Al_2C_3$, J. Appl. Phys. 113 (2013) 183519.

[8] M. Shamma, El'ad N. Caspi, B. Anasori, B. Clausen, D.W. Brown, S.C. Vogel, V. Presser, S. Amini, O. Yeheskel, M.W. Barsoum, In situ neutron diffraction evidence for fully reversible dislocation motion in highly textured polycrystalline Ti_2AlC bulks, Acta Mater. 98 (2015) 51-63.

[9] Z. Wang, G. Ma, Z. Li, H. Ruan, J. Yuan, L. Wang, P. Ke, A. Wang, Corrosion mechanism of Ti_2AlC MAX phase coatings under the synergistic effects of water vapor and solid NaCl at 600 °C. Corros. Sci. 192 (2021) 109788.

[10] Q.M. Wang, W. Garkas, A. Flores Renteria, C. Leyens, H.W. Lee, K.H. Kim, Oxidation behaviour of Ti-Al-C films composed mainly of a Ti_2AlC phase, Corros. Sci. 53 (9) (2011) 2948-2955.

[11] M. Sonestedt, J. Frodelius, M. Sundberg, L. Hultman, K. Stiller, Oxidation of Ti_2AlC bulk and spray deposited coatings, Corros. Sci. 52 (2010) 3955-3961.

[12] Z. Zhang, D.M.Y. Lai, S.H. Lim, J.W. Chai, S.J. Wang, H.M. Jin, J.S. Pan, Isothermal Oxidation of the Ti_2AlC MAX Phase Coatings Deposited by Kerosene-fuelled HVOF Spray, Corros. Sci. 138 (2018) 266-274.

[13] S. Basu, N. Obando, A. Gowdy, I. Karaman, M. Radovic, Long-term oxidation of Ti_2AlC in air and water vapor at 1000-1300 °C temperature range, J. Electrochem. Soc. 159 (2) (2012) C90-C96.

[14] M. Haftani, M.S. Heydari, H.R. Baharvandi, N. Ehsani, Studying the oxidation of Ti_2AlC MAX phase in atmosphere: A review, Int. J. Refract. Metals Hard Mater. 61 (2016) 51-60.

[15] D.J. Tallman, B. Anasori, M.W. Barsoum, A critical review of the oxidation of Ti_2AlC, Ti_3AlC_2 and Cr_2AlC in air, Mater. Res. Lett. 1 (3) (2013) 115-125.

[16] J. L. Smialek, Kinetic aspects of Ti_2AlC MAX phase oxidation, Oxid. Met. 83 (2015) 351-366.

[17] W. Yu, M. Vallet, B. Levraut, V. Gauthier-Brunet, S. Dubois, Oxidation mechanisms in bulk Ti_2AlC: Influence of the grain size, J. Eur. Ceram. Soc. 40 (5) (2020) 1820-1828.

[18] L.D. Xu, D.G. Zhu, Y.L. Liu, T.S. Suzuki, B.N. Kim, Y. Sakka, S. Grasso, C. Hu, Effect of texture on oxidation resistance of Ti_3AlC_2, J. Eur. Ceram. Soc. 38 (10)

(2018) 3417-3423.

[19] M.W. Barsoum, N. Tzenov, A. Procopio, T. El-Raghy, M. Ali, Oxidation of $Ti_{n+1}AlX_n$ (n=1-3 and X=C, N)-II. Experimental results, J. Electrochem. Soc. 148 (8) (2001) C551-C562.

[20] M.W. Barsoum, Oxidation of $Ti_{n+1}AlX_n$ (n=1-3 and X=C, N)-I. Model, J. Electrochem. Soc. 148 (8) (2001) C544-C550.

[21] X.Q. Li, X. Xie, J.G. Julian, Mechanical and oxidation behavior of textured Ti_2AlC and Ti_3AlC_2 MAX phase materials, J. Eur. Ceram. Soc. 30 (2020) 5258-5271.

[22] D.B. Lee, S.W. Park, High-temperature oxidation of Ti_3AlC_2 between 1173 and 1473 K in air, Mater. Sci. Eng. A 434 (1-2) (2006) 147-154.

[23] Z.Y. Wang, G.S. Ma, L.L. Liu, L. Wang, P.L. Ke, Q.J. Xue, A.Y. Wang. High-performance Cr_2AlC MAX phase coatings: Oxidation mechanisms in the 900-1100 °C temperature range. Corros. Sci. 167 (2020) 108492.

[24] J.L. Smialek, Oxygen diffusivity in alumina scales grown on Al-MAX phases, Corros. Sci. 91 (2015) 281-286.

[25] S. Lang, C. Fillmore, L. Maxwell, The system beryllia-alumina-titania: phase relations and general physical properties of three-component porcelains, J. Res. Nat. Bur. Stand. 48 (1952) 298-312.

[26] T. Ai, High-temperature oxidation behavior of un-dense Ti_3AlC_2 material at 1000 °C in air, Ceram. Int. 38 (3) (2012) 2537-2541.

[27] X.H. Wang, Y.C. Zhou, Oxidation behavior of Ti_3AlC_2 at 1000-1400 °C in air, Corros. Sci. 45 (5) (2003) 891-907.

[28] G.M. Song, V. Schnabel, C. Kwakernaak, S. van der Zwaag, J.M. Schneider, W.G. Sloof, High temperature oxidation behaviour of Ti_2AlC ceramic at 1200 °C, Mater. High. Temp. 29 (3) (2012) 205-209.

[29] B. Cui, D.D. Jayaseelan, W.E. Lee, TEM study of the early stages of Ti_2AlC oxidation at 900 °C, Scr. Mater. 67 (10) (2012) 830-833.

[30] M. Arita, M. Hosoya, M. Kobayashi, M. Someno, Depth profile measurement by secondary ion mass spectrometry for determining the tracer diffusivity of oxygen in rutile, J. Am. Ceram. Soc. 62 (9-10) (1979) 443-446.

[31] R. Haul, G. Dümbgen, Sauerstoff-selbstdiffusion in rutilkristallen, J. Phys. Chem. Solids 26 (1) (1965) 1-10.

[32] X.H. Wang, Y.C. Zhou, Oxidation behavior of TiC-containing Ti_3AlC_2 based material at 500-900 °C in air, Mater. Res. Innovat. 7 (6) (2003) 381-390.

[33] E. Drouelle, V. Gauthier-Brunet, J. Cormier, P. Villechaise, P. Sallot, F. Naimi, F. Bernard, S. Dubois, Microstructure-oxidation resistance relationship in Ti_3AlC_2 MAX phase, J. Alloys. Compd. 826 (2020) 154062.

[34] J. Zhang, J.Y. Wang, Y.C. Zhou, Structure stability of Ti_3AlC_2 in Cu and microstructure evolution of Cu-Ti_3AlC_2 composites, Acta Mater. 55 (13) (2007) 4381-4390.

[35] A. Rahmel, P. J. Spencer, Thermodynamic aspects of TiAl and $TiSi_2$ oxidation: The Al-Ti-O and Si-Ti-O phase diagrams, Oxid. Met. 35 (1-2) (1995) 53-68.

[36] J.C. Rao, Y.T. Pei, H.J. Yang, G.M. Song, S.B. Li, J.Th.M. De Hosson, TEM study of the initial oxide scales of Ti_2AlC, Acta Mater. 59 (2011) 5216-5223.

[37] N.S. Jacobson, M.P. Brady, G.M. Mehrotra, Thermodynamics of selected Ti-Al and Ti-Al-Cr alloys, Oxid. Met. 52 (5-6) (1999) 537-556.

[38] Y.X. Qin, W.J. Lu, D. Zhang, J.N. Qin, B. Ji, Oxidation of in situ synthesized TiC particle reinforced titanium matrix composites, Mater. Sci. Eng. A 404 (1-2) (2005) 42-48.

Figure Captions

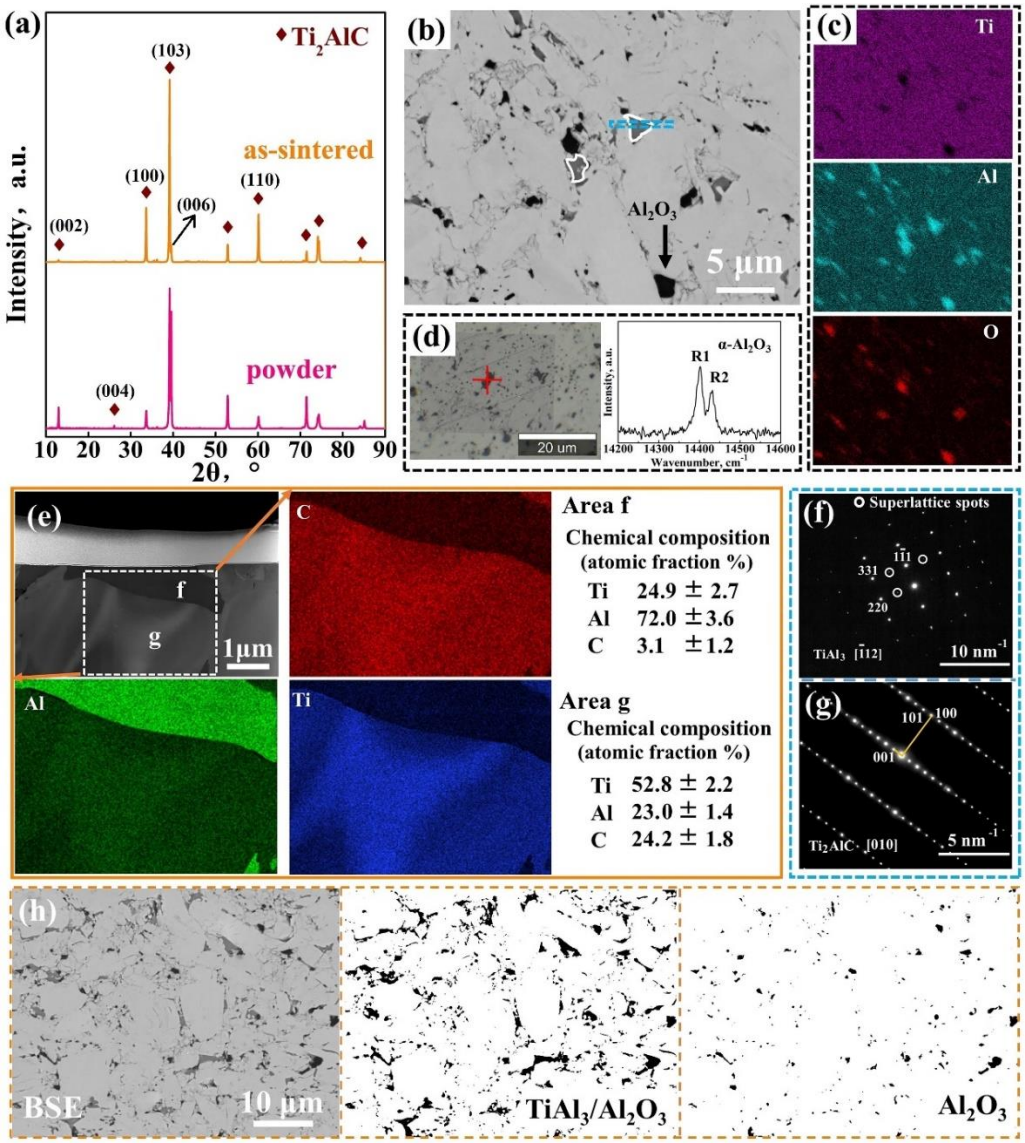

Fig. 1 Phase composition and microstructure of as-sintered Ti_2AlC samples: (a) XRD patterns of the Ti_2AlC powder and as-sintered sample; (b) BSE image of the polished surface of the Ti_2AlC sample; (c) Corresponding EDS mapping of (b); (d) An Al_2O_3 inclusion formed during sintering of Ti_2AlC powder; (e) STEM-HAADF image of the FIB lamella and the corresponding EDS analysis; (f and g) Selected-area diffraction patterns (SADPs) of the corresponding areas in (e); (h) Quantitative image analysis of volume fractions for $TiAl_3$ and Al_2O_3. Phase volume fraction is calculated from at least five polished surface morphology with a magnification of 5000× using the ImageJ software. The Blue rectangle in Fig. 1b represents a similar area where a FIB lamella was taken out.

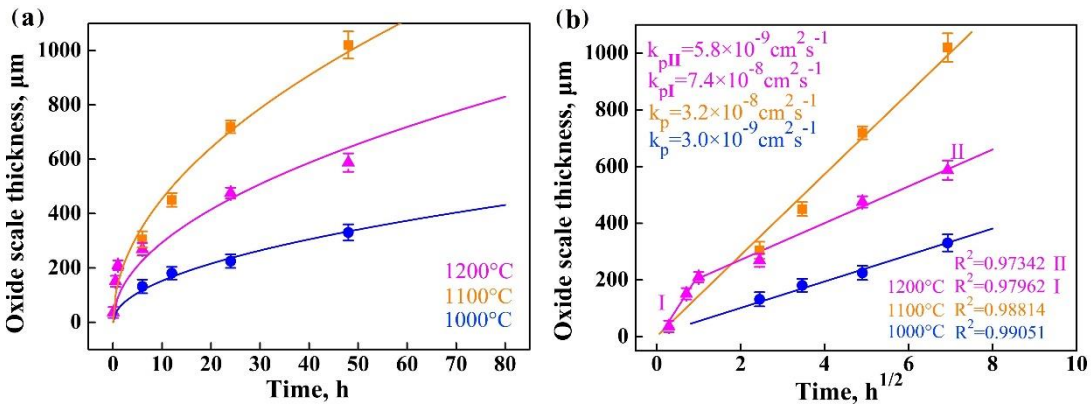

Fig. 2 The thickness of the oxide scale as a function of oxidation time (a) and square root of oxidation time (b), showing the parabolic law. The thickness of oxide scale is measured using ImageJ software based on the cross-sectional images of the oxide scale.

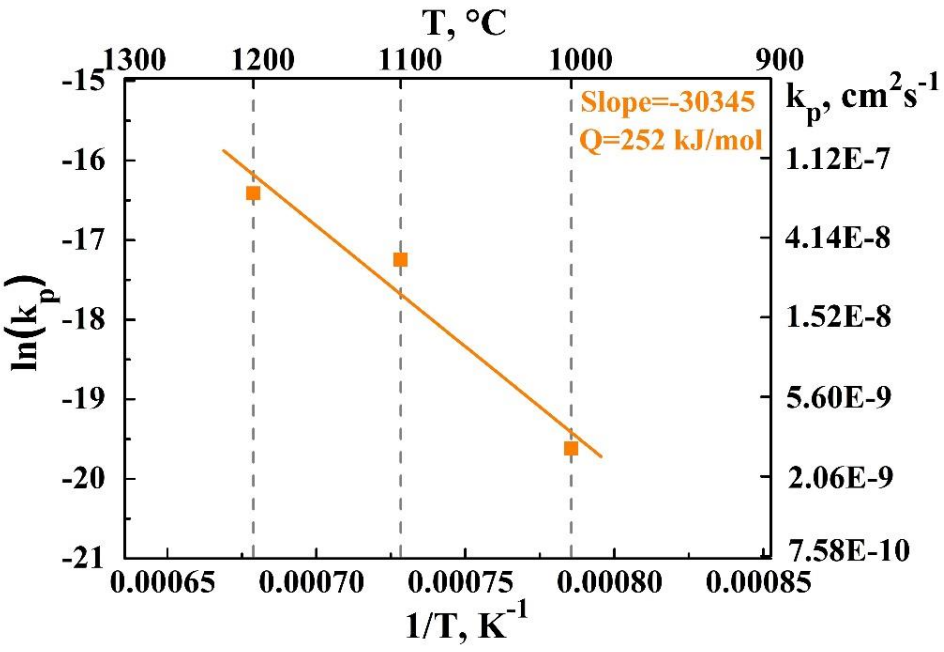

Fig. 3 Arrhenius-type plot as a function of 1/T.

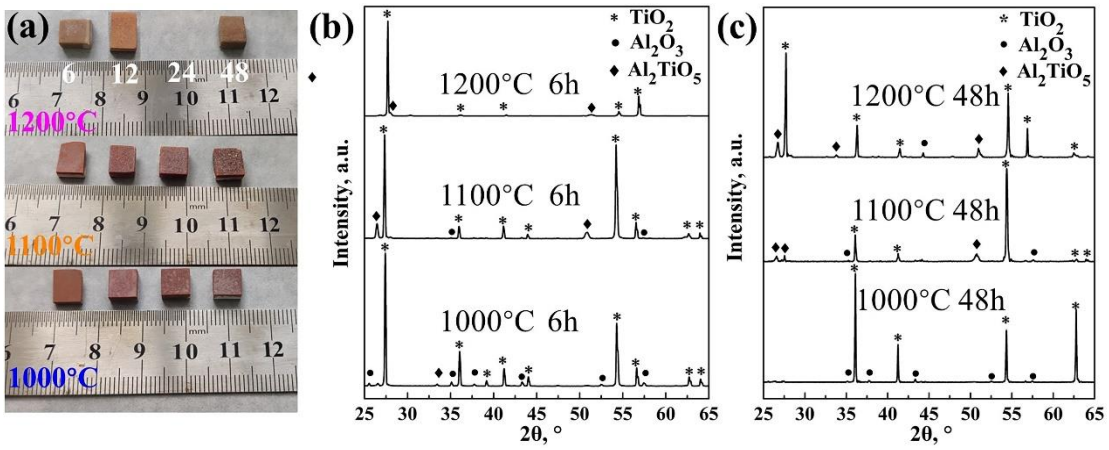

Fig. 4 (a) Surface appearance of Ti_2AlC samples after oxidation for 6, 12, 24 and 48 h, respectively; (b and c) XRD patterns of Ti_2AlC samples after oxidation for 6 and 48 h, respectively.

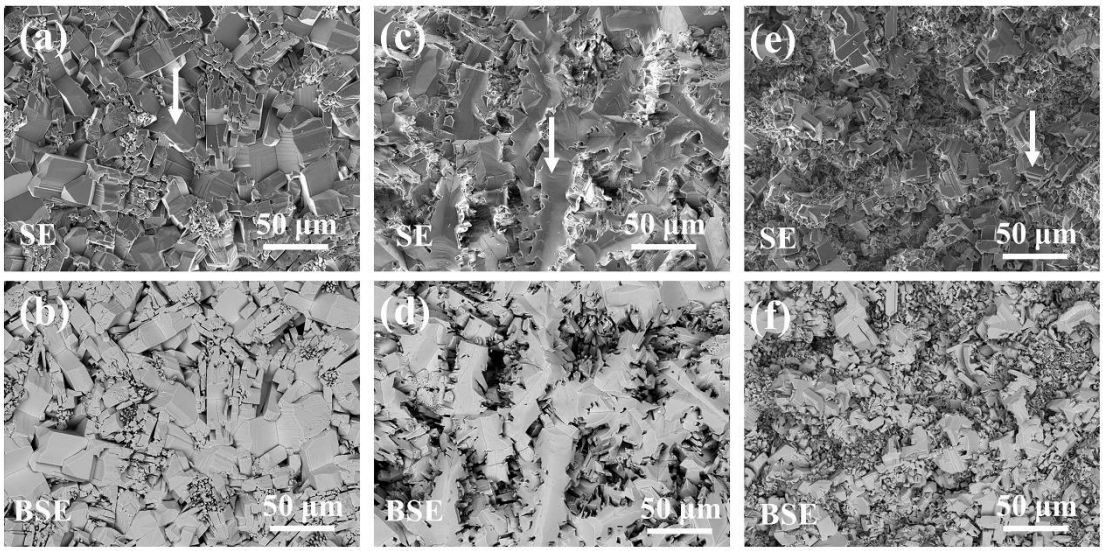

Fig. 5 Surface morphology of Ti_2AlC samples after oxidation for 48 h: (a and b) 1000 °C; (c and d) 1100 °C; (e and f) 1200 °C. Areas pointed by white arrows are rich in Ti and O.

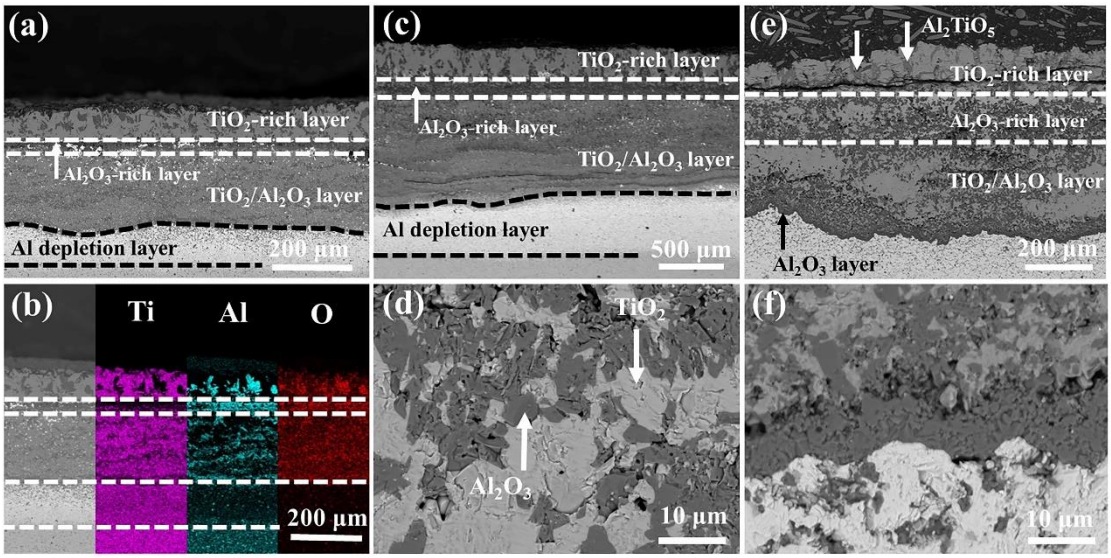

Fig. 6 Cross-sectional microstructure of oxide scales after 48 h oxidation at different temperatures: (a and b) 1000 °C; (c and d) 1100 °C; (e and f) 1200 °C. Fig. 6d shows the magnified area of the TiO_2/Al_2O_3 mixed layer in Fig. 6c. Fig. 6f shows the magnified area of the Al_2O_3 layer at the interface in Fig. 6e. The volume fraction of TiO_2 and Al_2O_3 in the TiO_2/Al_2O_3 mixed layer is calculated from at least three cross-sectional images using ImageJ software.

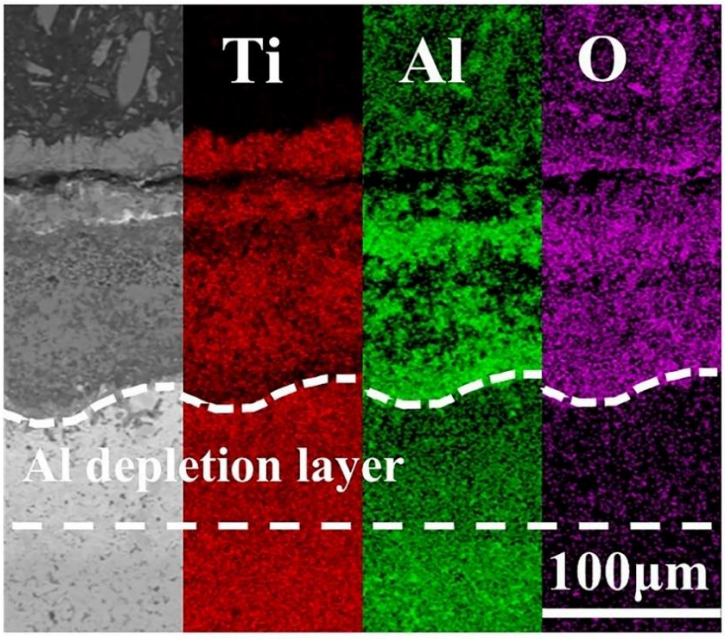

Fig. 7 The oxide scale formed on Ti_2AlC after 30 min oxidation at 1200 °C.

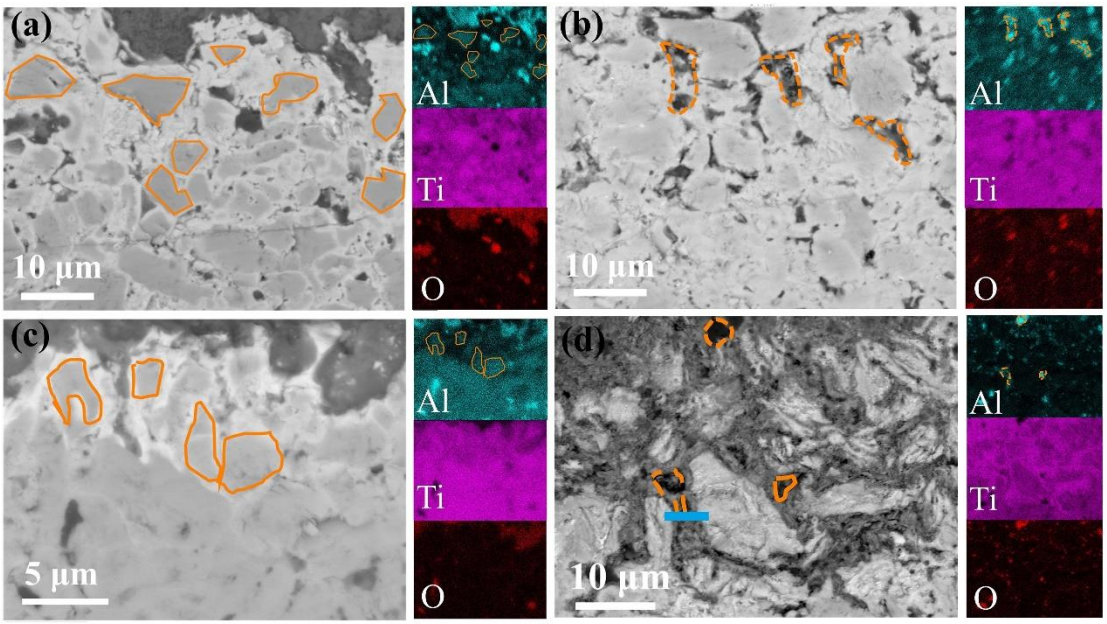

Fig. 8 High magnification images of the scale/substrate interface and corresponding EDS mapping after oxidation at (a) 1000 °C for 6 h; (b) 1100 °C for 6 h; (c) 1200 °C for 5 min and (d) 1200 °C for 30 min, respectively. Al-depletion areas highlighted by solid lines are along the edge of Ti_2AlC. Al_2O_3 is marked by dashed lines.

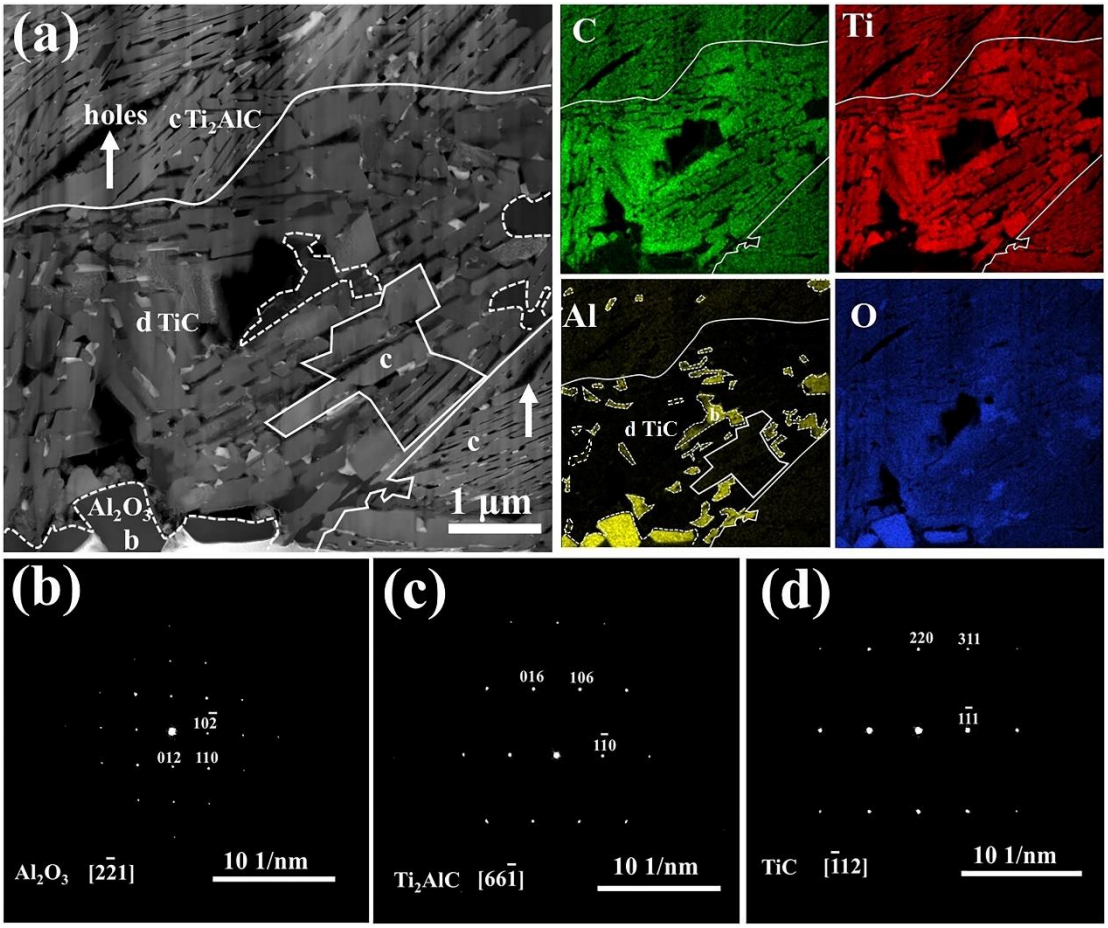

Fig. 9 (a) High-Angle Annular Dark Field (HAADF) STEM image and corresponding EDS mapping; Selected-area diffraction patterns (SADPs) of corresponding areas in (a): (b) Al_2O_3, (c) Ti_2Al_xC and (d) TiC. Region b (marked by dashed lines), c (marked by solid lines) and d are Al_2O_3, Ti_2Al_xC and TiC, respectively. Blue rectangle in Fig. 8d shows the area where the FIB lamella was extracted from.

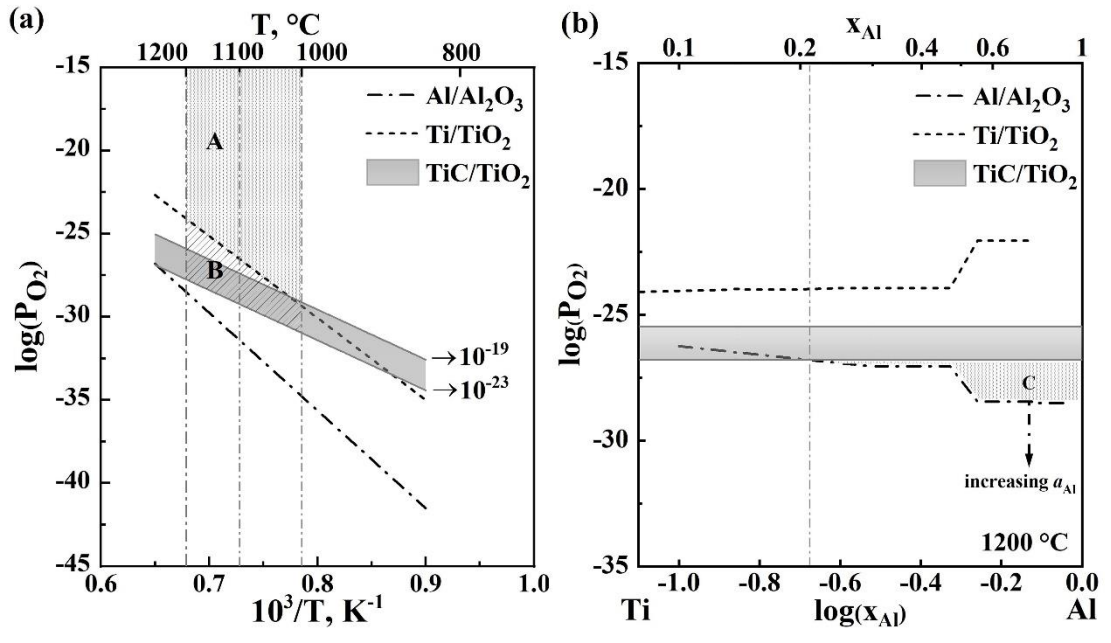

Fig. 10 (a) Oxygen equilibrium pressure of Al/Al_2O_3, Ti/TiO_2 and TiC/TiO_2.The activity of Al (a_{Al}) and Ti (a_{Ti}) is one. (b) Variation of the oxygen equilibrium pressure at 1200 °C. An assumption is made that the CO_2 partial pressure is about 10^{-23} to 10^{-19} bar. The vertical line in (b) denotes the Al content in Al-depleted Ti_2AlC.

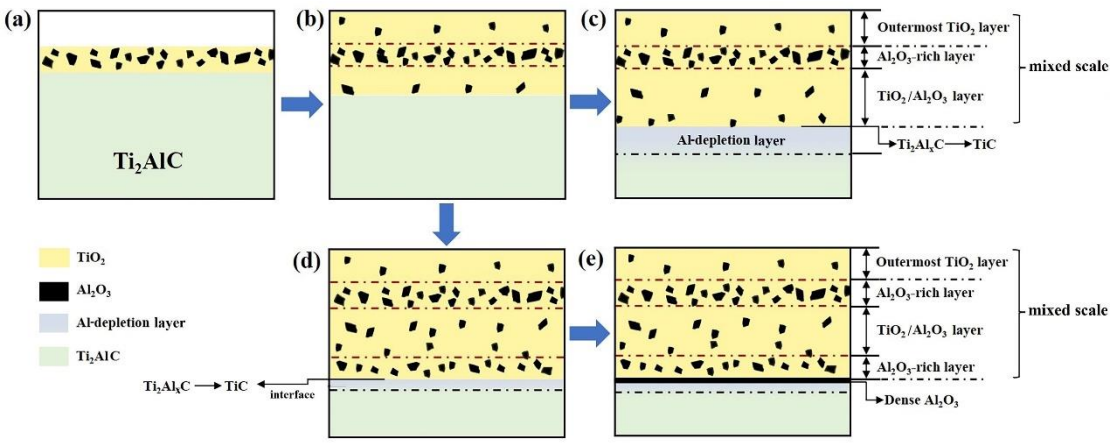

Fig. 11 Schematic illustration of the oxidation mechanism for Al-depleted Ti_2AlC at (a-c) 1000 °C and 1100 °C, (a, b, d and e) 1200 °C. Note that Al_2TiO_5 is not presented at the outermost TiO_2-rich layer due to its lower content compared with TiO_2 and Al_2O_3.